ARTICLE

Charge Transfer Dynamics in Conjugated Polymer/MoS_2 Organic/2D Heterojunctions

Received 00th January 20xx,
Accepted 00th January 20xx

DOI: 10.1039/x0xx00000x

Christopher E. Petoukhoff,*[a] Sofiia Kosar,[a] Manami Goto,[a] Ibrahim Bozkurt,[b] Manish Chhowalla,[b] and Keshav M. Dani[c]

Heterojunctions between organic and two-dimensional (2D) semiconductors show promising applications in ultrathin electronic and optoelectronic devices, including field-effect transistors, light-emitting diodes, and photovoltaics. These organic/2D heterojunctions form ideal interfaces due to the lack of dangling bonds at the surfaces of the neat (*i.e.*, individual) materials and their propensity to interact *via* van der Waals forces. Despite this, organic/2D heterojunction devices have had relatively low quantum efficiencies, suggesting limitations on the charge transport within these devices. Understanding the charge transfer dynamics across organic/2D semiconductor interfaces at fundamental time scales is an important part of overcoming these limitations. In this work, we investigate the photoexcited charge carrier dynamics in organic/2D heterojunctions comprised of large-area monolayer MoS_2 and solution-deposited organic semiconducting conjugated polymer thin-films. Using photoluminescence and femtosecond transient absorption spectroscopy, we compare the efficiencies of charge transfer for three different conjugated polymer/MoS_2 heterojunctions: P3HT, PCDTBT, and PTB7. We show that electron transfer occurs from MoS_2 to P3HT in under 9 ps, and from MoS_2 to PCDTBT or PTB7 in under 120 fs. Despite this, we demonstrate that the P3HT/MoS_2 heterojunction is the most efficient because the transferred charges have an order-of-magnitude increase in their lifetimes, giving rise to enhanced photoluminescence. This work will help guide designs of future organic/2D heterojunctions using scalable fabrication technologies.

Introduction

Semiconducting layered transition metal dichalcogenides (TMDCs) have received tremendous interest recently as novel optoelectronic materials with tuneable, thickness-dependent properties.[1-6] These layered TMDCs have weak inter-layer bonding held together by only van der Waals (vdW) forces, and so they can be exfoliated down to single monolayers, giving them two-dimensional (2D) behaviour. As monolayers, the optoelectronic properties of TMDCs behave vastly differently from their bulk forms – for instance, the exciton binding energy becomes several hundreds of meV, their bandstructures undergo an indirect-to-direct bandgap transition, and their absorption and photoluminescence efficiencies increase by orders of magnitude.[3-6] To exploit these unique properties of 2D TMDCs in functional optoelectronic devices, it is necessary to re-stack individual 2D layers of TMDCs to form vdW *p-n* heterojunctions.[7] 2D layers lack dangling bonds at their surfaces, enabling them to form ideal, defect-free interfaces without the need for energy-intensive growth processes, such as molecular beam epitaxy.[8] vdW heterojunctions have thus been employed in sub-nanometre-thick light-emitting diodes, photovoltaics, and photodetectors.[9-13] However, there are presently few routes towards fabricating large-area vdW heterostructures with high optoelectronic quality using only 2D materials.

Mixed-dimensional heterojunctions that are formed between 2D layers and materials of different dimensionality can overcome this issue due to the ease of scalability of the latter.[14] For optoelectronic applications, heterojunctions between organic (either 0D or 1D) and 2D semiconductors benefit from the processing technologies developed for the organic light-emitting diode (OLED) and organic photovoltaic (OPV) industries. Organic semiconductors also lack dangling bonds at their surfaces and interact *via* vdW forces, being ideal candidates to form *p-n* heterojunctions with 2D semiconductors.[8,15] Organic/2D heterojunctions have been employed as active *p-n* heterojunctions in optoelectronic devices such as photovoltaics and photodetectors,[8,15-20] as well as in field-effect transistors, demonstrating large on-off ratios and anti-ambipolar transfer characteristics.[21,22] For photovoltaic applications, organic semiconducting conjugated polymers are of particular interest due to their strong absorption coefficients in the visible regime, propensity to form uniform thin-films *via* solution-based processing techniques, and abundance of their elemental constituents.[23-27] Recently, conjugated polymer/2D heterojunctions fabricated from the polymer, poly([4,8-bis[(2-ethylhexyl)oxy]benzo[1,2-*b*:4,5-*b*']

[a] *Femtosecond Spectroscopy Unit, Okinawa Institute of Science and Technology Graduate University, Onna, Okinawa 904-0495, Japan. E-mail: christopher.petoukhoff@oist.jp*
[b] *Department of Materials Science and Engineering, Rutgers University, 607 Taylor Road, Piscataway, New Jersey 08854, United States.*
Electronic Supplementary Information (ESI) available: Transient absorption measurements at additional pump and probe wavelengths, fits to kinetic traces, and optical images of MoS_2 films. See DOI: 10.1039/x0xx00000x

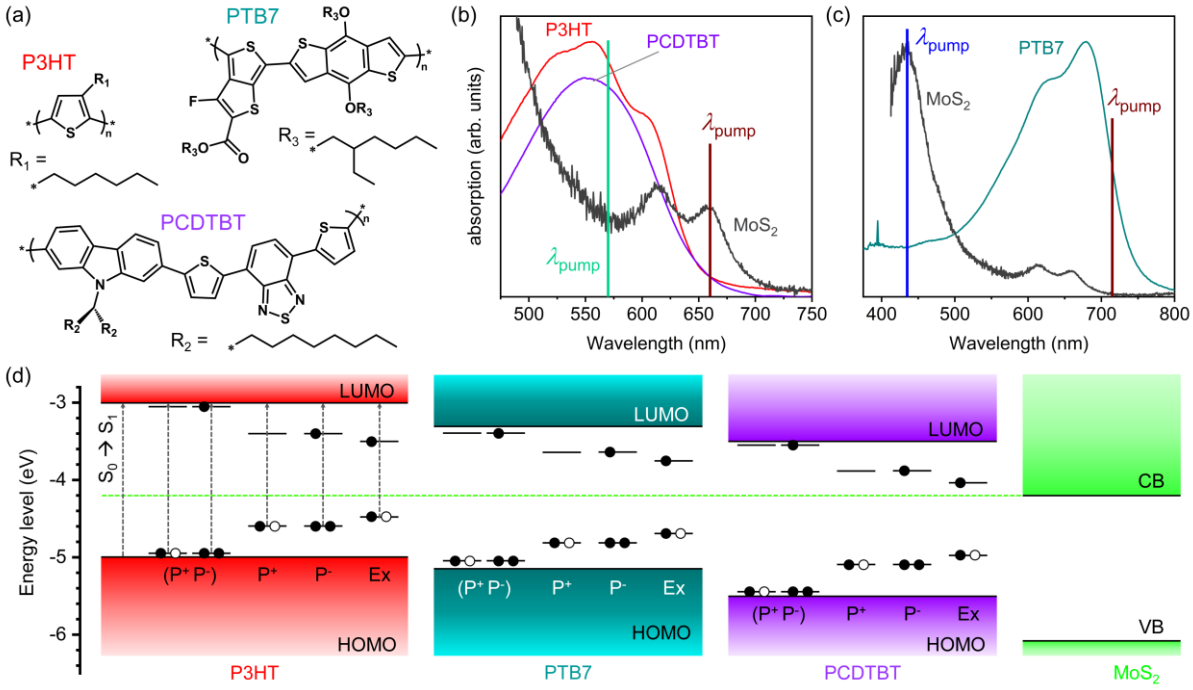

Fig. 1. (a) Molecular structures of the three conjugated polymers studied. (b,c) Ground-state absorption spectra of the neat conjugated polymer and MoS_2 films, with the different pump wavelengths labelled. In (b), the conjugated polymers have bandgap energies larger than that of MoS_2, whereas in (c), the conjugated polymer has a smaller bandgap energy than that of MoS_2. (d) Energy level diagrams of the three conjugated polymers and MoS_2. For MoS_2, only the conduction band (CB) and valence band (VB) edges are labelled.[4,16] For the three conjugated polymers, the ground state electronic bands are shaded in colours, and labelled as the highest occupied molecular orbital (HOMO) and lowest unoccupied molecular orbital (LUMO) bands.[36-38] In addition, the localized, photoinduced states are labelled within the bandgap as: polaron pairs [(P^+P^-)], positive polarons (P^+), negative polarons (P^-), and excitons (Ex).[39-48] Black dots represent electrons, whereas white dots represent holes. Transitions from the ground state (HOMO or S_0) and the different photoinduced levels to the first excited state (LUMO or S_1) are all indicated with dashed grey lines in the P3HT diagram only.

dithiophene-2,6-diyl][3-fluoro-2-[(2-ethylhexyl)carbonyl]thieno[3,4-*b*]thiophenediyl]) (PTB7), and the 2D material, MoS_2, have demonstrated the photovoltaic effect, with record values of the photovoltaic figures of merit normalized to the device active layer thickness.[28] Despite this, devices based on PTB7/MoS_2 heterojunctions have shown relatively low internal quantum efficiencies, suggesting non-ideal charge transport through the device. To-date, there have been limited investigations exploring the charge transport across organic/2D semiconductor interfaces, particularly at ultrafast timescales where electron dynamics occur.[29-31]

Here, we systematically investigate the photoexcited charge carrier dynamics within three different organic/2D heterojunctions based on thin-films of solution-processed conjugated polymers and chemical vapor deposited (CVD) MoS_2. MoS_2 has been used extensively in photovoltaic devices as either a charge transport layer or an active absorber layer.[8,11,15,32-34] The three conjugated polymers selected have been commonly employed in high-efficiency polymer:fullerene-based OPV devices, and so their photoexcitations have been well-studied.[35-37] We use polymers that give a range of different bandgap energies, while maintaining Type-II heterojunctions with MoS_2 (Figure 1), namely: regioregular poly(3-hexylthiophene-2,5-diyl) (P3HT); poly[N-9'-heptadecanyl-2,7-carbazole-*alt*-5,5-(4',7'-di-2-thienyl-2',1',3'-benzothiadiazole)] (PCDTBT); and PTB7 (Figure 1a). To investigate the photogenerated charge carrier dynamics within each of these organic/2D heterojunctions, we used a combination of photoluminescence and femtosecond transient absorption (TA) spectroscopies.

Results and Discussion

Organic/2D heterojunction design

The three conjugated polymers chosen gave a range of different bandgap energies and band alignment with MoS_2 (Figure 1b-d). Two of the polymers, P3HT and PCDTBT, have bandgap energies (~2 eV) larger than that of monolayer MoS_2 (1.9 eV). As such, MoS_2 can effectively broaden the absorption spectra of these polymers because its A-exciton resonance occurs at a longer wavelength (660 nm) than the absorption edge of these polymers (Figure 1b). Thus, by pumping the A-exciton resonantly, we should see an increase in the absorption transitions of the polymers if charge transfer from MoS_2 to the polymers occurs. To determine whether charge transfer from the polymers to MoS_2 occurs, we ideally need to pump only the polymers without exciting MoS_2. For P3HT/MoS_2 and PCDTBT/MoS_2, we pump the polymers near-resonance at 570 nm, which is non-resonant for MoS_2 (Figure 1b). However, since MoS_2 still absorbs at this wavelength, we employ a low bandgap polymer, PTB7, which has a bandgap energy of 1.85 eV, enabling

excitation of the polymer at 715 nm without causing photoexcitation in MoS_2 (Figure 1c).

The energy level diagram[4,16,36-38] in Figure 1d demonstrates that MoS_2 forms a Type-II heterojunction with each of the conjugated polymers. The main photoinduced states present in the conjugated polymers are labelled for each polymer, though for simplicity, the dominant optical transitions after photocarrier generation are labelled only for P3HT. These include the $S_0 \rightarrow S_1$ band-to-band transition, as well as photoinduced absorption by polaron pairs [*i.e.*, (P^+ P^-)], polarons (*i.e.*, P^+ or P^-), and excitons (*i.e.*, Ex).[39-48] Note that transitions from the highest occupied molecular orbital (HOMO) to the lower lying (P^+ P^-), P^+, P^-, and Ex states are also possible, but occur at wavelengths in the mid-IR, outside of our probe range. The transitions labelled in Figure 1d are the dominant transitions we probed using TA spectroscopy.

Photoluminescence spectroscopy

The photoluminescence (PL) spectra of the neat polymer films and polymer/2D heterojunctions, under 532 nm excitation, are shown in Figure 2. Changes in the PL spectra in the polymer/2D heterojunctions relative to the neat polymers can arise from three potential mechanisms: 1) charge transfer; 2) energy transfer; or 3) changes in the radiative recombination rate. We observed an enhancement in the PL signal in P3HT/MoS_2 relative to neat P3HT (Figure 2a), but quenching of the PL in PCDTBT/MoS_2 and PTB7/MoS_2 relative to the neat polymers (Figure 2b,c, respectively). This suggests that for P3HT/MoS_2, either charge or energy transfer occurred from MoS_2 to P3HT, or the radiative recombination rate of carriers in P3HT increased relative to neat P3HT. In the cases of PCDTBT/MoS_2 and PTB7/MoS_2, either charge or energy transfer from the polymers to MoS_2 occurred, or the radiative recombination rates of carriers in the polymers were reduced. Since the largest changes occurred for P3HT and PTB7, either P3HT or PTB7 formed the most efficient heterojunction with MoS_2, but understanding whether charge or energy transfer occurred in these organic/2D heterojunctions could not be resolved with PL alone.

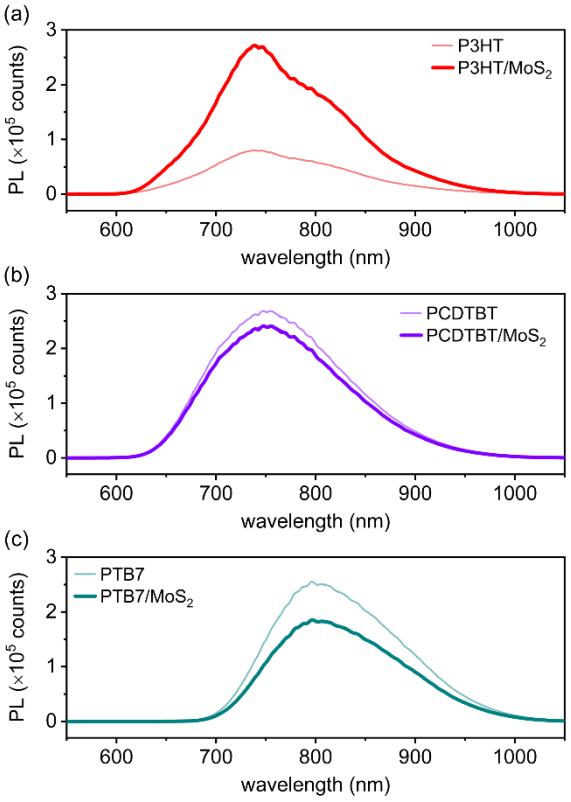

Fig. 2. Photoluminescence (PL) spectra from neat conjugated polymer films and conjugated polymer/MoS_2 heterojunctions. From top-to-bottom: (a) P3HT; (b) PCDTBT; and (c) PTB7. Spectra were acquired under 532 nm continuous-wave laser excitation with 1 mW average power.

TA spectroscopy of P3HT/MoS_2

To determine the nature of the PL enhancement and quenching observed in the conjugated polymer/MoS_2 heterojunctions, we employed femtosecond TA spectroscopy. TA spectroscopy is a versatile technique for determining charge and energy transfer in heterojunctions because, unlike in time-resolved PL, TA spectroscopy can probe both emissive and non-emissive states.[49] We first investigated P3HT/MoS_2 (Figure 3) by pumping the MoS_2 A-exciton resonantly (660 nm) and probing in the visible and NIR wavelengths. At an instant after photoexcitation, neat MoS_2 displayed its two characteristic A- and B- exciton features at 670 nm and 620 nm as bleach (negative) signals with photoinduced absorption (positive) signals centred at 500 nm and 708 nm (which has previously been attributed to from broadening of the exciton resonance in the excited state relative to the ground state)[50] (Figure 3a). Neat P3HT displayed its ground state bleach signals at 555 nm and 605 nm, and showed photoinduced absorption at 655 nm, which has been shown to arise from absorption by polaron pairs.[39,44,48] The TA spectrum of P3HT/MoS_2 displayed many of the same features as the neat P3HT and MoS_2 films; however, the spectrum was more than a simple addition of the spectra of MoS_2 and P3HT (Supplementary Information Figure S1a). The A- and B- exciton features observed in neat MoS_2 at 670 nm and 618 nm, respectively, were blue-shifted in the heterojunction to 664 nm and 607 nm. We attribute this blue-shift to a reduction in the exciton binding energy in the heterojunction due to dielectric screening from the polymer coatings.[30,51] Besides this spectral shift, there were three key differences in the spectrum of P3HT/MoS_2 relative to those of neat P3HT and MoS_2: an increase in the ground state bleach of P3HT at 550 nm; an increase in the total ground state bleach at 610 nm, and a decrease in the polaron pair absorption peak at 660 nm.

To understand these differences, we looked at the kinetic traces of P3HT/MoS_2, along with the neat P3HT and MoS_2 films, at these three wavelengths (Figure 3c-e). The bleach signal at 610 nm showed a marked increase in the signal in P3HT/MoS_2 relative to both neat films at all pump-probe time delays (Figure 3c). In fact, the bleach signal at 610 nm for P3HT/MoS_2 (-15.3×10^{-3}) was more than twice greater than the sum of the two neat films (-2.3×10^{-3} and -4.8×10^{-3}, for MoS_2 and P3HT,

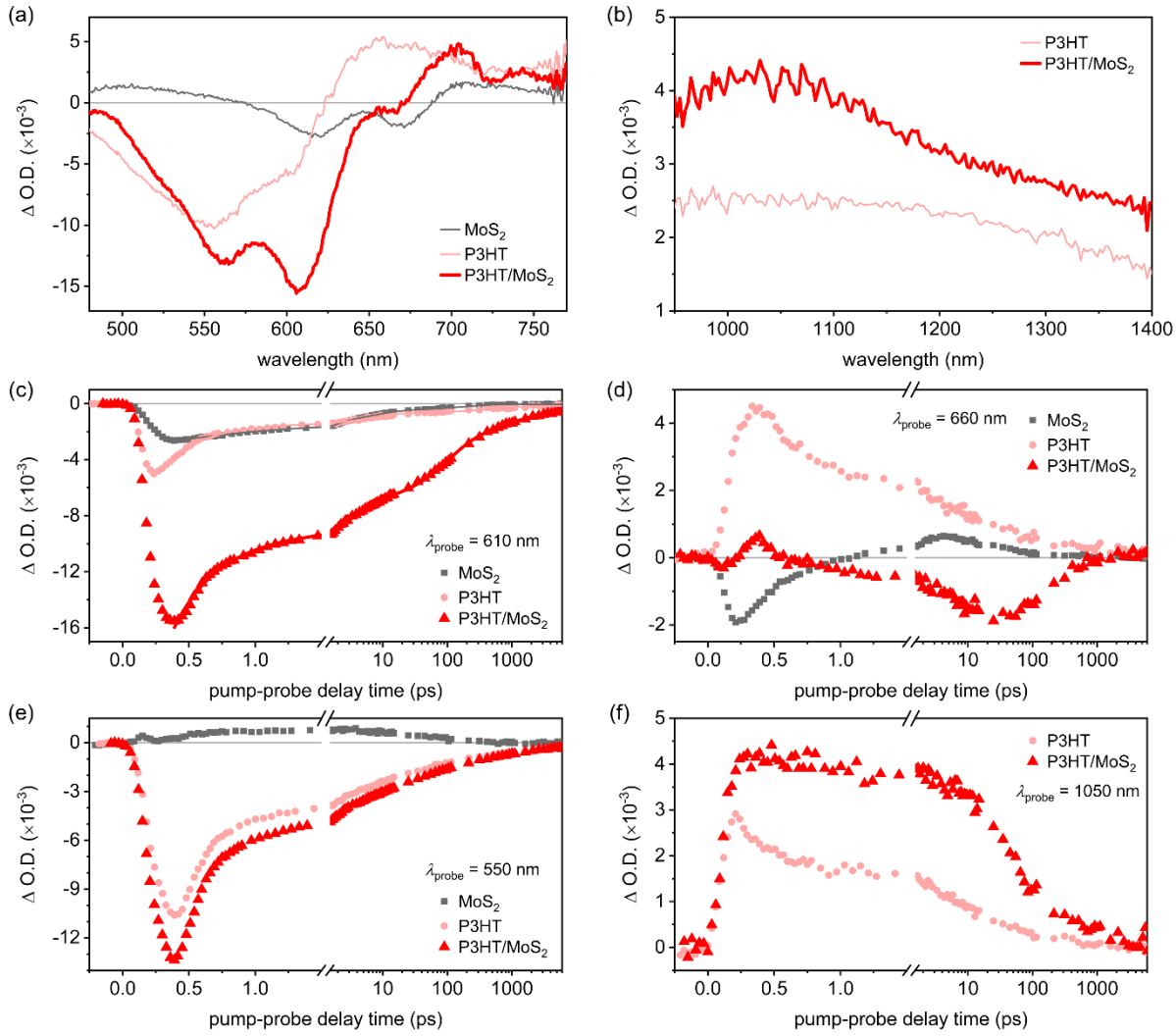

Fig. 3. Transient absorption (TA) spectra and kinetic traces for P3HT/MoS_2 and its neat constituents, with a pump wavelength of 660 nm and fluence of 61.2 μJ cm^{-2}. Visible (a) and near-infrared (b) spectra were taken at a pump-probe delay time of 270 fs. (c-f) Kinetic traces were extracted from the TA spectra at probe wavelengths of (c) 610 nm; (d) 660 nm; (e) 550 nm; and (f) 1050 nm.

respectively). The signal showed a rise time of about 200 fs for both MoS_2 and P3HT/MoS_2, and the decay dynamics followed along more closely to MoS_2 rather than to P3HT (Supplementary Information Figure S2). As such, we attribute the 610 nm bleach in P3HT/MoS_2 primarily to the ground state bleach signal of B-excitons in MoS_2, with minimal contributions from P3HT. This suggests that there was an additional pathway for decay of B-excitons before returning to the ground state, which, as we will show, was due to electron transfer from MoS_2 to P3HT.

The second wavelength that showed a pronounced change in P3HT/MoS_2 visible spectrum relative to the neat films was 660 nm, which is the wavelength of polaron pair photoinduced absorption in P3HT and the A-exciton ground state bleach in MoS_2 (Figure 3d). Unexpectedly, the signal from P3HT/MoS_2 showed completely different decay dynamics from either of the neat films, alternating between a bleach, followed by a photoinduced absorption, then another rising bleach, before relaxing back to the ground state. At 660 nm, MoS_2 showed a bleach signal at early timescales (less than 1 ps), then showed a rising photoinduced absorption signal up to 5 ps, before decaying back to the ground state. The rising photoinduced absorption signal came from broadening of the A-exciton resonance in the excited state.[50] P3HT showed a strong photoinduced absorption signal, with a maximum Δ O.D. of 5.1×10^{-3}, arising from absorption by polaron pairs.[39,44,48] However, P3HT/MoS_2 initially displayed a bleach signal within the first 120 fs, which decayed and rose to a photoinduced absorption signal within 390 fs, having a strength of 1.05×10^{-3}. The photoinduced absorption signal rapidly decayed to 0 within 600 fs, which was followed by a second rising bleach signal, reaching a maximum bleach of -1.88×10^{-3} by 25 ps, before decaying back to the ground state. The alternating bleach and photoinduced absorption signals suggest that the signal was initially a convolution of both the MoS_2 A-exciton bleach and the P3HT polaron pair absorption at time scale less than 390 fs. However, the population of polaron pairs in P3HT within the P3HT/MoS_2 heterojunction were reduced relative to neat P3HT, and their lifetime was reduced by several orders of magnitude,

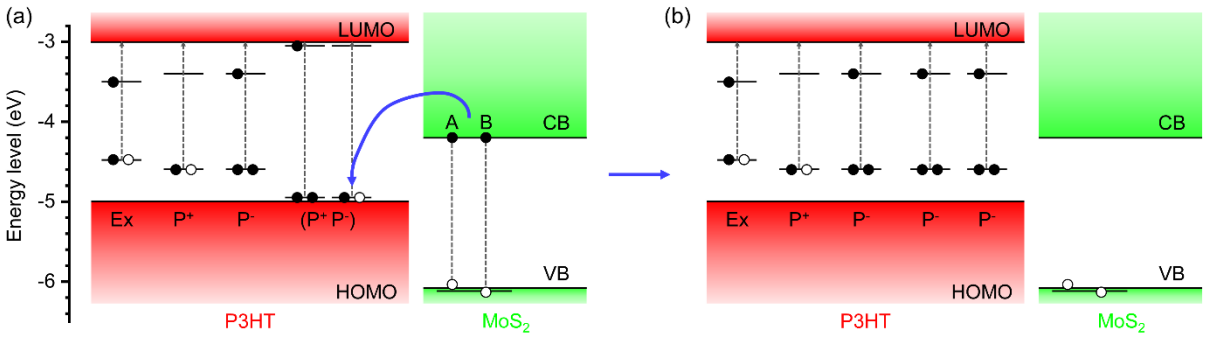

Fig. 4. Schematic showing proposed charge transfer process between MoS_2 and P3HT. (a) After photoexcitation, electrons in the conduction band of MoS_2 transfer to the lower lying hole of the polaron pair state in P3HT. (b) After recombining with the positive polaron from the polaron pair, excess negative polarons are left in P3HT, and the ground state of MoS_2 is left depleted.

from 290 ps to < 120 fs. At pump-probe time delays longer than 1 ps, we attribute the rising bleach signal to the ground state of MoS_2 becoming more depleted, turning the initially positive signal in the neat film into a bleach signal in P3HT/MoS_2. We attribute this to electron transfer from MoS_2 to P3HT polaron pair states, which occurred with a rise time of 9 ps (see Supplementary Information Figure S3 for fitting). We determined that electron transfer could not have taken place from MoS_2 directly to the HOMO of P3HT because the ground state bleach signal of P3HT at 550 nm increased from $–10.4\times10^{-3}$ in neat P3HT to $–13.2\times10^{-3}$ in P3HT/MoS_2 (Figure 3e). Thus, electrons from MoS_2 must have transferred to a photoexcited state in P3HT, such as polaron pairs, leaving the ground state more depleted.

So far, the data suggests that MoS_2 transferred electrons to P3HT polaron pair states, but we still do not know how polaron and exciton states changed in the P3HT/MoS_2 heterojunction relative to neat P3HT. To gain a more complete understanding of the charge transfer process, we took TA measurements in the NIR regime, where conjugated polymers have photoinduced absorption signals from polarons (~1000 nm) and excitons (~1300 nm)[48,52-55] (Figure 3b). The TA signals from P3HT/MoS_2 and neat P3HT in the NIR showed striking differences – P3HT/MoS_2 had a 1.7-fold increase in the signal at 1050 nm, and an overall broad spectral increase in the TA signal throughout the NIR relative to neat P3HT. We note that neat MoS_2 did not display a TA signal in the NIR. The polaron signal at 1050 nm was increased in P3HT/MoS_2 relative to neat P3HT for all pump-probe delay times (Figure 3f), and the decay time was slowed to 36 ps (562 ps) for the fast (slow) component compared to 3.8 ps (73 ps). Furthermore, the exciton signal at 1300 nm was only marginally increased in the P3HT/MoS_2 heterojunction and showed similar decay dynamics (Supplementary Information Figure S4). This shows that the P3HT polaron population was increased in the heterojunction, while the exciton population remained largely unchanged.

Description of charge transfer

Taking all of the probe wavelengths together, we make the following observations: 1) at 610 nm, the B-exciton bleach of MoS_2 increased by more than 2-fold compared to the sum of the bleach signals from the neat films; 2) at 660 nm, the population of polaron pairs in P3HT/MoS_2 reduced relative to neat P3HT, and the signal evolved into a bleach corresponding to the A-exciton bleach from MoS_2; 3) at 550 nm, the ground state bleach of P3HT increased slightly in P3HT/MoS_2 relative to neat P3HT; 4) at 1050 nm, the polaron population of P3HT increased a maximum of nearly 2-fold in P3HT/MoS_2 relative to neat P3HT, and showed an order-of-magnitude increase in lifetime; and 5) at 1300 nm, the exciton population of P3HT increased only marginally in P3HT/MoS_2. As such, we draw the following conclusions: electron transfer occurred from MoS_2 to P3HT via polaron pair states, accounting for the increased B- and A-exciton bleach signals in MoS_2 and the decreased polaron pair signal in P3HT (Figure 4a). Transferred electrons recombined with the holes in the polaron pair states, leaving behind the separated negative polarons, which gave rise to the increased polaron signal (Figure 4b). Because polaron pairs in P3HT tend to be interchain, trapped states, whereas excitons and polarons in P3HT are delocalized,[39,48] polaron pairs have a higher probability of recombination in the presence of excess, transferred electrons.

TA spectroscopy of PCDTBT/MoS_2 and PTB7/MoS_2

Having determined that the enhanced PL in P3HT/MoS_2 relative to neat P3HT arose from electron transfer from MoS_2 to P3HT, we next sought to determine the reason for the PL quenching in the PCDTBT and PTB7 organic/MoS_2 heterojunctions. TA spectra when resonantly pumping MoS_2 and probing in the visible regime showed similar behaviour for the PCDTBT and PTB7 neat films and heterojunctions (Figure 5a,d). Neat PCDTBT displayed its ground state bleach centred at 580 nm, and a broad photoinduced absorption peak centred at 668 nm (Figure 5a). PCDTBT/MoS_2 displayed two strong bleach signals at 620 nm and 670 nm, which were both significantly enhanced relative to the sum of signals between the neat films (Supplementary Information Figure S1b). The kinetic traces at these two wavelengths (Figure 5b,c) showed similar decay dynamics as the MoS_2 B- and A-excitons, respectively, suggesting that the dominant contribution to these signals arose from MoS_2 excitons. The remaining signals in PCDTBT/MoS_2 showed the same behaviour as P3HT/MoS_2:

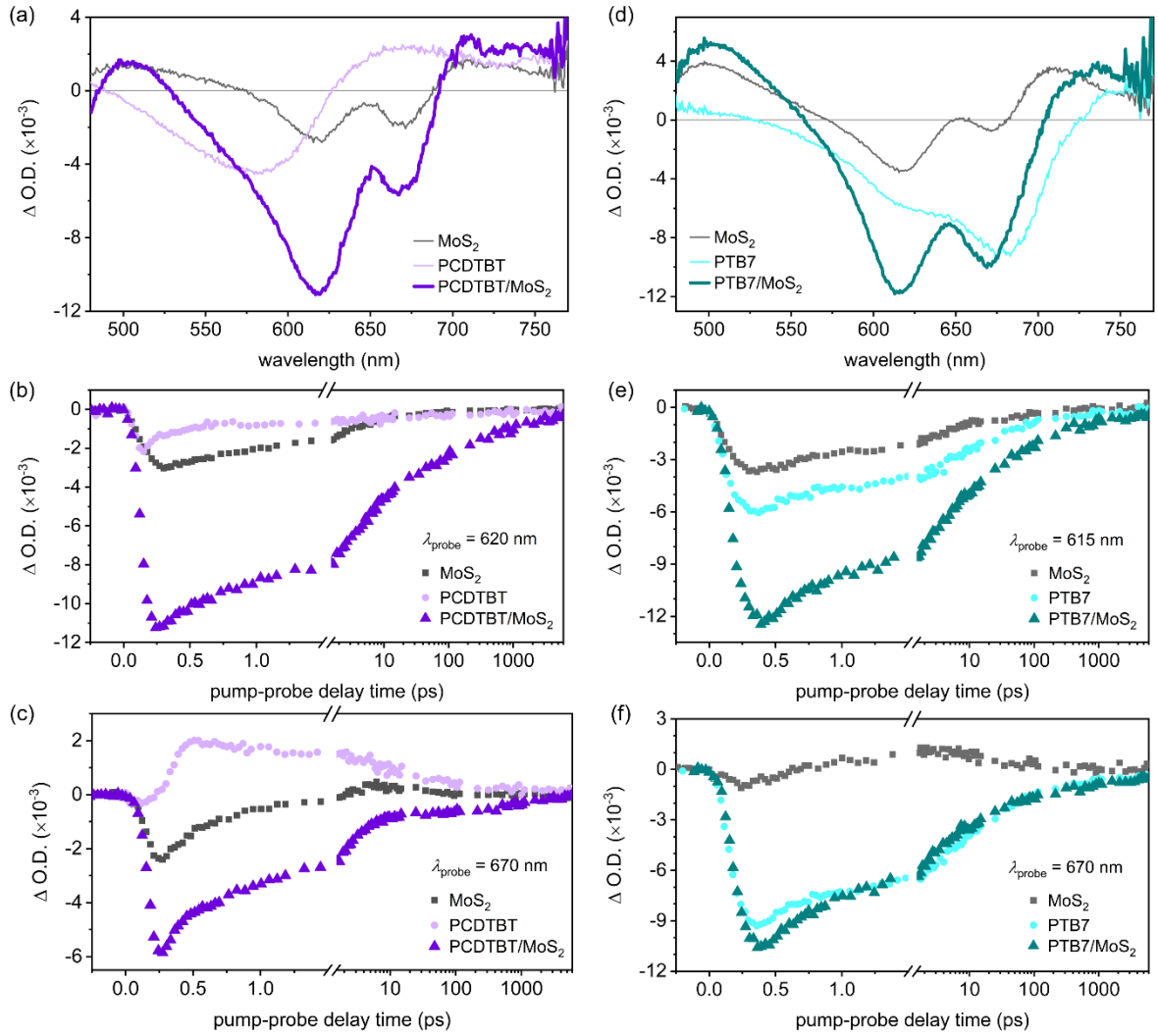

Fig. 5. Transient absorption (TA) spectra and kinetic traces for (a-c) PCDTBT/MoS_2 and (d-f) PTB7/MoS_2 heterojunctions and their neat constituents with a pump wavelength of 660 nm and fluence of 61.2 μJ cm^{-2}. (a,d) Visible spectra were taken at a pump-probe delay time of 270 fs. Kinetic traces were extracted from the TA spectra at probe wavelengths of (b) 620 nm and (c) 670 nm for PCDTBT/MoS_2; and (e) 615 nm and (f) 670 nm for PTB7/MoS_2.

increase in the ground state bleach of PCDTBT at 580 nm; increase in the polaron photoinduced absorption at 1000 nm; and negligible change in the exciton signal at 1300 nm (Supplementary Information Figure S5). As such, we concluded that PCDTBT/MoS_2 behaved in the same manner as P3HT/MoS_2: electron transfer from MoS_2 to PCDTBT polaron pair states occurred, this time in under 120 fs, due to the lack of a rise signal in the A-exciton bleach at 670 nm. PTB7/MoS_2 again showed the same general trends (Figure 5d-f and Supplementary Information Figure S6) as PCDTBT, only for this heterojunction, the only signal that was enhanced over the sum of signals of the neat films in the visible regime was at 615 nm (Supplementary Information Figure S1c).

Polaron lifetimes

We have shown that for P3HT, PCDTBT, and PTB7 organic/MoS_2 heterojunctions, MoS_2 transferred electrons from its exciton states to the polaron pair states in the polymers. In the case of P3HT, this resulted in enhanced PL (Figure 2a); however, this did not explain the quenched PL in PCDTBT/MoS_2 and PTB7/MoS_2 (Figure 2b,c). We did not observe any evidence of charge or energy transfer from the polymers to MoS_2 when selectively photoexciting the polymers (Supplementary Information Figures S7-S9). However, the recombination rates of the emissive polaron states changed from neat polymers to the polymer/MoS_2 heterojunctions (Figure 6). In all three polymer/MoS_2 heterojunctions, the polaron photoinduced absorption signal at ~1000 nm was increased relative to the neat polymers (Figure 6a). The lifetimes of the polarons were different with or without the MoS_2 for all polymers. Each of the kinetic traces were fit with a sum of 2-3 exponential decays (Supplementary Information Table S1). We compared the two dominant decay components with or without MoS_2 (Figure 6b). For P3HT, the lifetimes increased from 3.8 ps (73 ps) to 36 ps (562 ps) for the fast (slow) component with the addition of MoS_2. However, the lifetimes decreased with the addition of MoS_2 for PCDTBT and PTB7: for PCDTBT, the lifetimes decreased

from 6.5 ps (99 ps) to 3.1 ps (75 ps) for the fast (slow) component; for PTB7, the lifetimes decreased from 2.6 ps (57 ps) to 1.6 ps (24 ps) for the fast (slow) component. We attribute the quenching of the PL in PCDTBT/MoS_2 and PTB7/MoS_2 to the decreased lifetime of the polaron states, which arose from increased non-radiative recombination pathways. The PL was enhanced in P3HT/MoS_2 due to the order-of-magnitude increase in the polaron lifetimes, resulting in increased radiative recombination. We propose that the reason for the differences between P3HT and PCDTBT or PTB7 polymer/MoS_2 heterojunctions was due to the crystallinity of the 3 polymers: regio-regular P3HT forms a semi-crystalline polymer film,[56,57] whereas PCDTBT and PTB7 are both amorphous polymer films.[58-61] Since P3HT polarons are delocalized along the crystalline domains,[39,43,48] they tend to have longer lifetimes and lower non-radiative recombination pathways. Polarons within the amorphous polymers are more localized, and thus have a higher fraction of non-radiative recombination. Thus, although electron transfer from MoS_2 to the conjugated polymers occurred in each heterojunction, the P3HT/MoS_2 heterojunction was the most efficient due to the increased lifetime of the transferred charges.

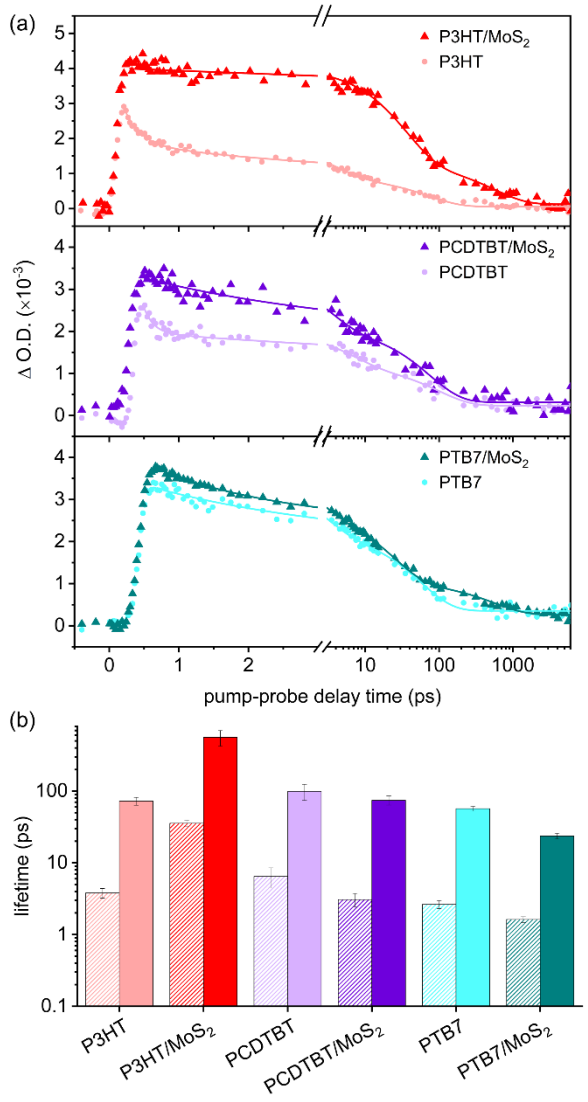

Fig. 6. (a) Kinetic traces of the polaron photoinduced absorption signals centred at wavelengths of 1050 nm (P3HT) or 1000 nm (PCDTBT and PTB7), with multiexponential decay fits overlaid. Pump wavelength was 660 nm and fluence was 61.2 μJ cm^{-2}. (b) Decay constants extracted from multiexponential fits for each of the neat conjugated polymers and conjugated polymer/MoS_2 heterojunctions. The first, striped bar in each group is the fast decay component, and the second, solid bar in each group is the slow component.

Conclusions

In this work, we have investigated the charge transfer dynamics between monolayer MoS_2 and three different conjugated polymers within organic/2D heterojunctions. We observed enhanced photoluminescence for the P3HT/MoS_2 organic/2D heterojunction relative to neat P3HT, but quenched photoluminescence for the PCDTBT/MoS_2 and PTB7/MoS_2 heterojunctions. Using transient absorption spectroscopy, we showed that electron transfer from MoS_2 excitons to polaron pairs within the three different conjugated polymers occurred within 9 ps for P3HT, and within 120 fs for PCDTBT and PTB7. We showed that the enhancement or quenching in the photoluminescence arose from either an increase or decrease in the lifetime of emissive polaron states, respectively. We suggest that P3HT/MoS_2 should serve as a more efficient organic/2D heterojunction than PCDTBT/MoS_2 or PTB7/MoS_2, and that when designing Type-II organic/2D heterojunctions using conjugated polymers, care is taken to select polymers that support delocalized polarons. Further exploring the mechanisms of charge transfer in the most efficient of the three heterojunctions, namely P3HT/MoS_2, by tuning other parameters, such as pump excitation intensity, is the subject of on-going studies.

Experimental

Organic/2D Heterojunction Fabrication

Large-area, polycrystalline single-layer MoS_2 films were grown on SiO_2/Si substrates by chemical vapor deposition (CVD) as described previously.[29] MoS_2 films were transferred to fused silica substrates using thermal release tape (TRT, Nitto, Revalpha No. 3196).[62] This was done by applying the TRT to MoS_2 films and applying pressure for 1 h; next, the substrate was immersed in water and sonicated for 15 minutes to disrupt the adhesion between the MoS_2 and the substrate. Once the tape separated from the substrate, it was dried using compressed nitrogen before being transferred to the fused silica substrate. Pressure was applied for another 1 h before heating the new substrate to 100 °C to remove the tape. Optical maps, SEM, AFM, Raman, and PL spectra of transferred MoS_2 films are in the Supplementary Information (Figures S11-S13).

Conjugated polymer solutions were prepared with 10 g/L concentration. Regioregular P3HT (Rieke Metals, product number: 4002-E) and PTB7 (1 Material, product number: OS0007) were both separately dissolved in chlorobenzene;

PCDTBT (Lumtec, product number: LT-S948P1) was dissolved in *o*-dichlorobenzene. The solutions were all heated to 60 °C and stirred rapidly for 60 min; PCDTBT solution was additionally heated to 90 °C and stirred rapidly for an additional 60 min. All solutions were filtered using 0.2 μm PTFE membranes, then spin-coated at 6000 rpm onto either fused silica substrates or onto transferred MoS2 films. Polymer films were ~20 nm thick, as confirmed using surface profilometry and were uniform over large areas (Supplementary Information Figure S10). After spin-coating, all samples were coated with epoxy (Norland Optical Adhesive, NOA 68) and covered with another fused silica superstrate to minimize air exposure during measurements. Epoxy was cured under a UV lamp for 15 min.

Photoluminescence Measurements

Photoluminescence (PL) measurements were conducted using a microscope-coupled spectrometer (Tokyo Instruments Nanofinder 30) with a 50× microscope objective (*N.A.* = 0.8). Samples were excited using a 532 nm CW diode-pumped solid-state laser with 1 mW average power. Fluorescence from the samples was collected through a 500 μm pinhole and dispersed by a 100 groove/mm grating onto the cooled CCD.

Transient Absorption Spectroscopy

Transient absorption (TA) measurements were conducted using a 1 kHz, 800 nm, 70 fs Ti:sapphire regenerative amplifier laser system (Spectra-Physics Spitfire ACE). Pump pulses were generated using optical parametric amplification (TOPAS) from 1 mJ of the fundamental wavelength. The pump wavelength was chosen to selectively excite either MoS_2 (660 nm or 435 nm) or the conjugated polymers (570 nm or 715 nm), depending on the relative bandgap energy of the polymers to that of MoS_2 (Figure 1b,c). A portion of the 800 nm beam was focused through either a sapphire or YAG crystal to generate white light in the visible (450 nm to 750 nm) or NIR (900 nm to 1600 nm) regime, respectively, which was then focused onto the sample at a spot size of 790 μm and was used to probe the change in absorption (Δ O.D.) in the heterojunctions. The probe light was collected through a fibre and coupled to a spectrometer (Newport TAS). The pump was chopped at 500 Hz, which was synced to the spectrometer to allow for collection of the O.D. of the probe in both the absence and presence of the pump at each time delay. Fluences of 61.2 μJ cm^{-2} and 4.1 μJ cm^{-2} were chosen when pumping MoS_2 and the conjugated polymers, respectively, which generated at least 10^{18} excitons/cm^3 for each material selectively excited. For all measurements, at least 25 scans were averaged to achieve reasonable signal-to-noise ratio. The cross-correlation of the pump and probe at the sample position gave a temporal full-width half max of 120 fs.

Conflicts of interest

There are no conflicts to declare.

Acknowledgements

This work was supported in part by funding from the Femtosecond Spectroscopy Unit, Okinawa Institute of Science and Technology Graduate University. The authors thank Vivek Pareek, Takaaki Harada, and M. Bala Murali Krishna for useful discussions.

Notes and references

1 M. Chhowalla, H. S. Shin, G. Eda, L.-J. Li, K. P. Loh and H. Zhang, *Nat. Chem.*, 2013, **5**, 263-275.
2 S. Das, J. A. Robinson, M. Dubey, H. Terrones and M. Terrones, *Annu. Rev. Mater. Res.*, 2015, **45**, 1-27.
3 G. Eda, H. Yamaguchi, D. Voiry, T. Fujita, M. Chen and M. Chhowalla, *Nano Lett.*, 2011, **11**, 5111-5116.
4 K. F. Mak, C. Lee, J. Hone, J. Shan and T. F. Heinz, *Phys. Rev. Lett.*, 2010, **105**, 136805:136801-136804.
5 A. Splendiani, L. Sun, Y. Zhang, T. Li, J. Kim, C.-Y. Chim, G. Galli and F. Wang, *Nano Lett.*, 2010, **10**, 1271-1275.
6 J. W. Park, H. S. So, S. Kim, S.-H. Choi, H. Lee, J. Lee, C. Lee and Y. Kim, *J. Appl. Phys.*, 2014, **116**, 183509:183501-183506.
7 A. K. Geim and I. V. Grigorieva, *Nature*, 2013, **499**, 419-425.
8 D. Jariwala, S. L. Howell, K. S. Chen, J. Kang, V. K. Sangwan, S. A. Filippone, R. Turrisi, T. J. Marks, L. J. Lauhon and M. C. Hersam, *Nano Lett.*, 2016, **16**, 497-503.
9 H.-M. Li, D. Lee, D. Qu, X. Liu, J. Ryu, A. Seabaugh and W. J. Yoo, *Nat. Commun.*, 2015, **6**, 6564.
10 M. Bernardi, M. Palummo and J. C. Grossman, *Nano Lett.*, 2013, **13**, 3664-3670.
11 Y. Deng, Z. Luo, N. J. Conrad, H. Liu, Y. Gong, S. Najmaei, P. M. Ajayan, J. Lou, X. Xu and P. D. Ye, *ACS Nano*, 2014, **8**, 8292-8299.
12 M. M. Furchi, A. Pospischil, F. Libisch, J. Burgdörfer and T. Mueller, *Nano Lett.*, 2014, **14**, 4785-4791.
13 J. Yuan, S. Najmaei, Z. Zhang, J. Zhang, S. Lei, P. M. Ajayan, B. I. Yakobson and J. Lou, *ACS Nano*, 2015, **9**, 555-563.
14 D. Jariwala, T. J. Marks and M. C. Hersam, *Nat. Mater.*, 2017, **16**, 170-181.
15 F. Liu, W. L. Chow, X. He, P. Hu, S. Zheng, X. Wang, J. Zhou, Q. Fu, W. Fu, P. Yu, Q. Zeng, H. J. Fan, B. K. Tay, C. Kloc and Z. Liu, *Adv. Funct. Mater.*, 2015, **25**, 5865-5871.
16 L.-Y. Gan, Q. Zhang, Y. Cheng and U. Schwingenschlögl, *J. Phys. Chem. Lett.*, 2014, **5**, 1445-1449.
17 D. He, Y. Pan, H. Nan, S. Gu, Z. Yang, B. Wu, X. Luo, B. Xu, Y. Zhang, Y. Li, Z. Ni, B. Wang, J. Zhu, Y. Chai, Y. Shi and X. Wang, *Appl. Phys. Lett.*, 2015, **107**, 183103.
18 R. Chen, C. Lin, H. Yu, Y. Tang, C. Song, L. Yuwen, H. Li, X. Xie, L. Wang and W. Huang, *Chem. Mater.*, 2016, **28**, 4300-4306.
19 H. Zhang, J. Choi, A. Ramani, D. Voiry, S. N. Natoli, M. Chhowalla, D. R. McMillin and J. H. Choi, *ChemPhysChem*, 2016, **17**, 2854-2862.
20 M. Sun, P. Yang, D. Xie, Y. Sun, J. Xu, T. Ren and Y. Zhang, *Adv. Electron. Mater.*, 2019, **5**, 1800580.
21 H. J. Park, C. J. Park, J. Y. Kim, M. S. Kim, J. Kim and J. Joo, *ACS Appl. Mater. Interfaces*, 2018, **10**, 32556-32566.
22 J. Yan, Y. Hao, Y. Cui, J. Zhang, Y. Zou, W. Zhang, G. Yu, J. Zheng, W. Xu and D. Zhu, *J. Mater. Chem. C*, 2018, **6**, 12976-12980.
23 R. D. McCullough, *Advanced materials*, 1999, **10**, 93-116.
24 J. Roncali, *Chem. Rev.*, 1992, **92**, 711-738.
25 Y.-J. Cheng, S.-H. Yang and C.-S. Hsu, *Chem. Rev.*, 2009, **109**, 5868-5923.
26 F. C. Krebs, *Sol. Energy Mater. Sol. Cells*, 2009, **93**, 394-412.
27 E. Nakamura and K. Sato, *Nat. Mater.*, 2011, **10**, 158-161.
28 T. A. Shastry, I. Balla, H. Bergeron, S. H. Amsterdam, T. J. Marks and M. C. Hersam, *ACS Nano*, 2016, **10**, 10573-10579.

29 C. E. Petoukhoff, M. B. M. Krishna, D. Voiry, I. Bozkurt, S. Deckoff-Jones, M. Chhowalla, D. M. O'Carroll and K. M. Dani, *ACS Nano*, 2016, **10**, 9899-9908.
30 S. B. Homan, V. K. Sangwan, I. Balla, H. Bergeron, E. A. Weiss and M. C. Hersam, *Nano Lett.*, 2017, **17**, 164-169.
31 C. Zhong, V. K. Sangwan, C. Wang, H. Bergeron, M. C. Hersam and E. A. Weiss, *J. Phys. Chem. Lett.*, 2018, **9**, 2484-2491.
32 X. Gu, W. Cui, H. Li, Z. Wu, Z. Zeng, S.-T. Lee, H. Zhang and B. Sun, *Adv. Energy Mater.*, 2013, **3**, 1262-1268.
33 M. Shanmugam, T. Bansal, C. A. Durcan and B. Yu, *Appl. Phys. Lett.*, 2012, **100**, 153901:153901-153904.
34 M.-L. Tsai, S.-H. Su, J.-K. Chang, D.-S. Tsai, C.-H. Chen, C.-I. Wu, L.-J. Li, L.-J. Chen and J.-H. He, *ACS Nano*, 2014, **8**, 8317-8322.
35 G. Li, V. Shrotriya, J. Huang, Y. Yao, T. Moriarty, K. Emery and Y. Yang, *Nat. Mater.*, 2005, **4**, 864-868.
36 S. H. Park, A. Roy, S. Beaupré, S. Cho, N. Coates, J. S. Moon, D. Moses, M. Leclerc, K. Lee and A. J. Heeger, *Nat. Photonics*, 2009, **3**, 297-303.
37 Z. He, C. Zhong, S. Su, M. Xu, H. Wu and Y. Cao, *Nat. Photonics*, 2012, **6**, 591-595.
38 C. E. Petoukhoff, D. K. Vijapurapu and D. M. O'Carroll, *Sol. Energy Mater. Sol. Cells*, 2014, **120**, 572-583.
39 O. J. Korovyanko, R. Österbacka, X. M. Jiang, Z. V. Vardeny and R. A. J. Janssen, *Phys. Rev. B*, 2001, **64**, 235122.
40 R. Tautz, E. Da Como, T. Limmer, J. Feldmann, H.-J. Egelhaaf, E. von Hauff, V. Lemaur, D. Beljonne, S. Yilmaz, I. Dumsch, S. Allard and U. Scherf, *Nat. Commun.*, 2012, **3**, 970.
41 C. Enengl, S. Enengl, S. Pluczyk, M. Havlicek, M. Lapkowski, H. Neugebauer and E. Ehrenfreund, *ChemPhysChem*, 2016, **17**, 3836-3844.
42 E. M. Conwell and H. A. Mizes, *Phys. Rev. B*, 1995, **51**, 6953-6958.
43 R. Österbacka, C. P. An, X. M. Jiang and Z. V. Vardeny, *Science*, 2000, **287**, 839-842.
44 Y. H. Kim, D. Spiegel, S. Hotta and A. J. Heeger, *Phys. Rev. B*, 1988, **38**, 5490-5495.
45 M. J. Nowak, S. D. D. V. Rughooputh, S. Hotta and A. J. Heeger, *Macromolecules*, 1987, **20**, 965-968.
46 A. J. Heeger, *Chem. Soc. Rev.*, 2010, **39**, 2354-2371.
47 W. R. Salaneck, R. H. Friend and J. L. Brédas, *Phys. Rep.*, 1999, **319**, 231-251.
48 J. Guo, H. Ohkita, H. Benten and S. Ito, *J. Am. Chem. Soc.*, 2009, **131**, 16869-16880.
49 R. Berera, R. van Grondelle and J. T. Kennis, *Photosynth. Res.*, 2009, **101**, 105-118.
50 S. Sim, J. Park, J.-G. Song, C. In, Y.-S. Lee, H. Kim and H. Choi, *Phys. Rev. B*, 2013, **88**, 075434.
51 E. A. Pogna, M. Marsili, D. De Fazio, S. Dal Conte, C. Manzoni, D. Sangalli, D. Yoon, A. Lombardo, A. C. Ferrari, A. Marini, G. Cerullo and D. Prezzi, *ACS Nano*, 2016, **10**, 1182-1188.
52 J. Cabanillas-Gonzalez, G. Grancini and G. Lanzani, *Adv. Mater.*, 2011, **23**, 5468-5485.
53 K. Yonezawa, H. Kamioka, T. Yasuda, L. Han and Y. Moritomo, *Appl. Phys. Express*, 2012, **5**, 042302.
54 J. M. Szarko, B. S. Rolczynski, S. J. Lou, T. Xu, J. Strzalka, T. J. Marks, L. Yu and L. X. Chen, *Adv. Funct. Mater.*, 2014, **24**, 10-26.
55 B. S. Rolczynski, J. M. Szarko, H. J. Son, Y. Liang, L. Yu and L. X. Chen, *J. Am. Chem. Soc.*, 2012, **134**, 4142-4152.
56 R. J. Kline, M. D. McGehee, E. N. Kadnikova, J. Liu, J. M. J. Fréchet and M. F. Toney, *Macromol.*, 2005, **38**, 3312-3319.
57 R. J. Kline, M. D. McGehee and M. F. Toney, *Nat. Mater.*, 2006, **5**, 222-228.
58 Z. M. Beiley, E. T. Hoke, R. Noriega, J. Dacuña, G. F. Burkhard, J. A. Bartelt, A. Salleo, M. F. Toney and M. D. McGehee, *Adv. Energy Mater.*, 2011, **1**, 954-962.
59 P. A. Staniec, A. J. Parnell, A. D. F. Dunbar, H. Yi, A. J. Pearson, T. Wang, P. E. Hopkinson, C. Kinane, R. M. Dalgliesh, A. M. Donald, A. J. Ryan, A. Iraqi, R. A. L. Jones and D. G. Lidzey, *Adv. Energy Mater.*, 2011, **1**, 499-504.
60 M. R. Hammond, R. J. Kline, A. A. Herzing, L. J. Richter, D. S. Germack, H.-W. Ro, C. L. Soles, D. A. Fischer, T. Xu, L. Yu, M. F. Toney and D. M. DeLongchamp, *ACS Nano*, 2011, **5**, 8248-8257.
61 J. M. Szarko, J. Guo, Y. Liang, B. Lee, B. S. Rolczynski, J. Strzalka, T. Xu, S. Loser, T. J. Marks, L. Yu and L. X. Chen, *Adv. Mater.*, 2010, **22**, 5468-5472.
62 Y. Tsuboi, F. Wang, D. Kozawa, K. Funahashi, S. Mouri, Y. Miyauchi, T. Takenobu and K. Matsuda, *Nanoscale*, 2015, **7**, 14476-14482.